ADVANCED OPTICAL MATERIALS

www.advopticalmat.de

A Broadband Optical Diode for Linearly Polarized Light Using Symmetry-Breaking Metamaterials

Minkyung Kim, Kan Yao, Gwanho Yoon, Inki Kim, Yongmin Liu, and Junsuk Rho**

As an analog of electrical diodes, optical diodes enable asymmetric transmission or one-way transmission of light. Here, a thin bilayer metamaterial supporting asymmetric transmission is experimentally demonstrated for linearly polarized light but not for circularly polarized light over a broad bandwidth up to 50 terahertz in the near-infrared region. A simple and intuitive working principle based on the symmetry inherent in the metamaterial design is provided, along with full-wave simulations that agree well with the experimental results. It is also proved that the design is extremely insensitive to spatial misalignment, which may occur during the nanofabrication process. These prominent features promise a wide range of applications, such as ultrafast optical computing, information processing, and suppressing undesired interactions of light in integrated micro- and nanodevices.

There has been rapidly growing interest in optical-diode phenomena, meaning light can transmit through a material or device along one direction but not the opposite direction. Such a property is fundamentally interesting because light transmission is normally symmetric due to the Lorentz reciprocity in time-invariant linear media. In order to break the Lorentz symmetry condition, which requires the scattering matrix to be asymmetric, we can employ magneto-optical materials,[1,2] nonlinear media,[3] or spatial–temporal modulations of refractive indices.[4,5] All the three approaches could implement an ideal optical isolator that can transmit and block any spatial mode in the opposite two directions. However, these approaches are quite challenging, especially at the integrated and complementary metal-oxide semiconductor (CMOS) compatible system level.

Metamaterials, engineered materials with extraordinary optical properties originated from subwavelength structures, provide an alternative simple solution to realize optical diodes via mode conversion between specific modes, even though the system is completely reciprocal. The underlying mechanism arises from the spatial symmetry breaking. Different reciprocal optical diodes have been proposed and demonstrated by employing various metamaterials and metasurfaces. For instance, asymmetric transmission for circularly polarized light has been realized by chiral metamaterials including split-ring resonator and fish-scale patterns.[6–11] Asymmetric transmission of linear polarization has been also reported using asymmetric gratings,[12,13] grating-patterned metal–dielectric bilayer[14] and metal–dielectric multilayer,[15] and specifically designed unit cell including bilayer metallic strips,[16] half-gammadions,[17] a U-shaped resonator,[18–20] and L-shaped bilayer structures.[21,22] However, the reported structures are rather narrow band or limited to GHz range which is not favorable for optical applications, or they have low asymmetric transmission value, near one fifth. It should be noted that reciprocal optical diodes have also been demonstrated in the realm of photonic crystals[23–26] and parity-time symmetric waveguide.[27–29] In addition, it is worth mentioning that strong polarization conversion by metamaterials has been demonstrated in the terahertz region,[30,31] which potentially could be scaled to the optical wavelengths to realize broadband asymmetric transmission.

In this paper, we present numerical and experimental demonstrations of an optical metamaterial composed of two layers of half-gammadion structures for asymmetric transmission of linearly polarized light with up to 50 THz bandwidth in the short-wavelength infrared region. We have developed microscopic dipolar description to unveil the fundamental mechanism of the asymmetric transmission. Furthermore, the performance is highly robust even under misalignment errors, which might take place in the fabrication process. Our research findings promise novel applications such as on-chip optical computing, information communication, and prevention of unwanted interferences and interactions in integrated photonic circuits.

M. Kim, G. Yoon, I. Kim, Prof. J. Rho
Department of Mechanical Engineering
Pohang University of Science and Technology (POSTECH)
Pohang 37673, Republic of Korea
E-mail: jsrho@postech.ac.kr

K. Yao, Prof. Y. Liu
Department of Electrical and Computer Engineering
Northeastern University
Boston, MA 02115, USA
E-mail: y.liu@northeastern.edu

Prof. Y. Liu
Department of Mechanical and Industrial Engineering
Northeastern University
Boston, MA 02115, USA

Prof. J. Rho
Department of Chemical Engineering
Pohang University of Science and Technology (POSTECH)
Pohang 37673, Republic of Korea

Prof. J. Rho
National Institute of Nanomaterials Technology (NINT)
Pohang 37673, Republic of Korea

DOI: 10.1002/adom.201700600

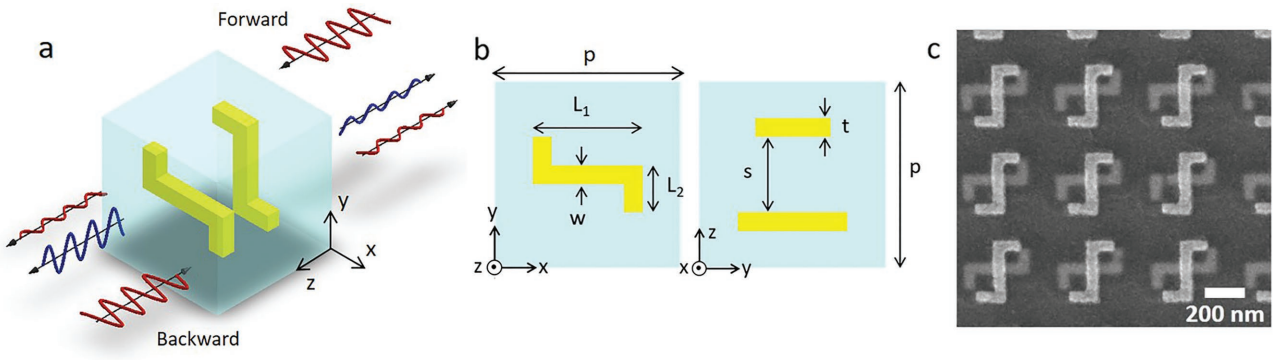

Figure 1. Schematics of the unit cell and SEM image of the fabricated device. a) Perspective view of the unit cell of the proposed metamaterial. Two layers of half-gammadion structures made of gold are embedded in SiO_2. Propagation direction is defined as forward for the +*z*-direction and backward for the −*z*-direction. The metamaterial shows different transmission characteristics for forward and backward *x*-polarized incidence via polarization state conversion. b) Top view of the upper half-gammadion structures (left) and side view of the unit cell (right) with geometrical parameters indicated in the figure: $p = 500$ nm, $L_1 = 350$ nm, $L_2 = 150$ nm, $s = 200$ nm, $w = 60$ nm, $t = 50$ nm. c) SEM image of the fabricated device.

Figure 1a shows the perspective view of a unit cell of the metamaterial, which consists of two layers of periodic gold half-gammadion structures embedded in a silica substrate. The two layers have a 200 nm spacing distance to break symmetry in the propagation direction. With respect to the bottom layer, the upper layer is rotated by an angle of $\pi/2$ about the *z*-axis and then rotated π about the *y*-axis. Figure 1b illustrates the geometry of the metamaterial, while the scanning electron microscope (SEM) image of one fabricated device is presented in Figure 1c.

The conditions of asymmetric transmission for linearly polarized light can be examined through Jones calculus. Jones matrix, whose components have complex values, transforms Jones vector of the incident field $\begin{pmatrix} I_x \\ I_y \end{pmatrix}$ to that of transmitted field $\begin{pmatrix} T_x \\ T_y \end{pmatrix}$.[32,33] Mathematically, it follows

$$\begin{pmatrix} T_x \\ T_y \end{pmatrix} = T_f \begin{pmatrix} I_x \\ I_y \end{pmatrix}, \text{ with } T_f = \begin{pmatrix} T_{xx} & T_{xy} \\ T_{yx} & T_{yy} \end{pmatrix} \quad (1)$$

where T_f represents Jones matrix for the forwad propagation direction (along the +*z*-axis). From the Lorentz reciprocity theorem,[34] Jones matrix for the backward propagation direction (along the −*z*-axis) has the following form

$$T_b = \begin{pmatrix} T_{xx} & -T_{yx} \\ -T_{xy} & T_{yy} \end{pmatrix} \quad (2)$$

Asymmetric transmission, denoted as Δ, is defined as the difference between transmittance in the forward direction and transmittance in the backward direction. It can be readily proved that the asymmetric transmission for *x*- and *y*-polarized light is given by

$$\Delta_{(x)} = |T_{yx}|^2 - |T_{xy}|^2 = -\Delta_{(y)} \quad (3)$$

In order to achieve asymmetric transmission, first of all, the spatial symmetry of the metamaterials along the propagation direction should be broken; otherwise, transmission along the forward and the backward propagation direction is symmetric. Secondly, on the basis of the changing process of the circularly polarized light, one can conclude that transmission coefficients should satisfy $T_{xx} = T_{yy}$ and $|T_{xy}| \neq |T_{yx}|$ to exhibit asymmetric transmission for linear polarization only, but not for circular polarization.[33] Since the unit cell of the proposed metamaterial is symmetric under $\pi/2$ rotation about the *z*-axis followed by π rotation about the *y*-axis, i.e., invariant under $R_y(\pi)R_z(\pi/2)$, *x*-polarized incidence in the forward propagation direction is equivalent to *y*-polarized incidence in the backward propagation direction. Therefore, the Jones matrix of the backward propagation is equal to the Jones matrix of the forward propagation after the two rotation transformations. In other words

$$\begin{pmatrix} T_{xx} & -T_{yx} \\ -T_{xy} & T_{yy} \end{pmatrix} = \Im \begin{pmatrix} T_{xx} & T_{xy} \\ T_{yx} & T_{yy} \end{pmatrix} \Im^{-1}, \text{ with } \Im = \begin{pmatrix} 0 & -1 \\ 1 & 0 \end{pmatrix} \quad (4)$$

Such a symmetry described by Equation (4) ensures $T_{xx} = T_{yy}$. On the other hand, because the unit cell of the designed metamaterial lacks fourfold rotational symmetry, the structure is anisotropic. This results in different crosspolarization conversion coefficients; i.e., $|T_{xy}| \neq |T_{yx}|$. Therefore, the proposed metamaterials enable asymmetric transmission to occur only for linearly polarized light, providing additional degrees of freedom in photonics applications, since we do not need to use additional quarter-wave plates to generate and detect circularly polarized light.

We have performed numerical simulations based on commercial electromagnetic solver (CST Microwave Studio) to validate our design. In the simulation, we have used the Drude model to describe gold with plasma frequency 1.367×10^{16} rad s^{-1} and collision frequency 4.0715×10^{13} rad s^{-1}. The simulation results are plotted as solid lines in **Figure 2**. The transmission of light through the device is normalized by the transmission through a bare silica substrate. One can see that in the forward direction, a large portion of *x*-polarized incident light is converted to *y*-polarized transmitted waves, resulting in large T_{yx}, while the *x*-polarized component of the transmitted light is negligible, producing small T_{xx} (Figure 2a). In a sharp contrast, for the backward propagating case, *x*-polarized incident light has very low transmission, that is, both T_{xx} and T_{yx} are small (Figure 2b).

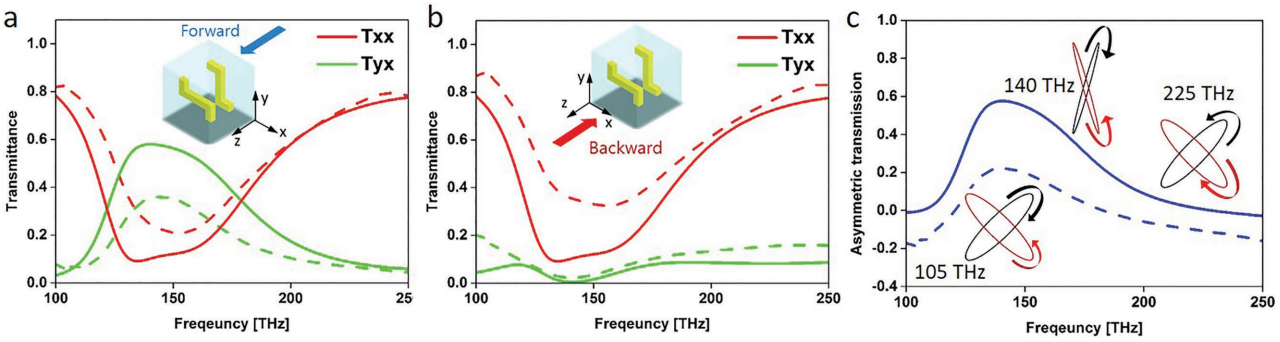

Figure 2. The simulated (solid line) and the measured (dashed line) transmittance under *x*-polarized incidence. a) Transmittance for forward propagation. b) Transmittance for backward propagation. c) Asymmetric transmission of *x*-polarized light. The insets show eigen-polarization states of forward propagation at three different frequencies retrieved from simulated transmission spectra.

Note that coefficient T_{xx} is identical for both forward and backward directions. These results clearly show that transmittance along the forward and the backward propagation direction is different, giving rise to asymmetric transmission spanning a broad range from 125 to 175 THz (Figure 2c). Here, only the transmittance for *x*-polarized incidence is presented, but the transmittance of *y*-polarized light can be easily obtained from the relations between Jones matrices. Specifically, the transmission coefficient of *y*-polarized light under *y*-polarized illumination (T_{yy}) is same for both propagation directions, and it satisfies and $T_{yy} = T_{xx}$ as expected from Equation (4). The cross-polarized transmission coefficient T_{xy}, instead, shows distinct behavior for both forward and backward propagations.

We have fabricated large-scale (100 μm × 100 μm) bilayer half-gammadion metamaterials using electron beam lithography. The SEM image of a device is shown in Figure 1c. Fused silica is used as a substrate, and 3 nm chrome is deposited as an adhesion layer under 50 nm thick gold half-gammadion structures. Then the transmittance spectra of the fabricated device are measured using Fourier transform infrared spectroscopy (FTIR). The experimental results are plotted as dashed lines in Figure 2, which show very good agreement with the simulations. We have fabricated three different devices and confirmed that the measured transmittance is all consistent to the simulated one. The decreased asymmetric transmission contrast in the experiment is mainly attributed to the imperfection in the fabrication such as geometry deviation of the fabricated devices from the design. More details about the fabrication process and optical measurement can be found in the Supporting Information.

The underlying mechanism of asymmetric transmission arises from the different nonorthogonal eigen-polarization states of the symmetry-breaking metamaterials. Here, we discuss the correlation between asymmetric transmission and orthogonality of eigen-polarization states. Through the same analysis as Equation (4), we can deduce that a structure that is symmetric along the propagation axis has $\begin{pmatrix} A & B \\ B & D \end{pmatrix}$ type of Jones matrix. Therefore, the Jones matrix of forward propagation and that of backward propagation share the same set of eigenvectors. Jones matrix of the bilayer half-gammadion metamaterial, however, has a form of $\begin{pmatrix} A & B \\ C & A \end{pmatrix}$. In such a case, eigenvalues of forward propagation and those of backward propagation are identical but eigenvectors are not identical anymore.

Assuming $e_1 = (1\ a)^T$ and $e_2 = (b\ 1)^T$ are the two distinct (unnormalized) eigen-polarization states where $a, b \in \mathbb{C}$ and $ab \neq 1$, then, a and b are determined by solving the eigenvalue problem. More specifically, we can obtain

$$a^2 = 1/b^2 = C/B \tag{5}$$

Since $ab \neq 1$, b is equal to $-1/a$. Now normalizing the two eigenstates and expressing them with real-valued parameters, we can obtain

$$e_1 = \left(\alpha\ \beta e^{i\phi}\right)^T, e_2 = \left(\alpha\ -\beta e^{i\phi}\right)^T$$
$$\alpha = \frac{1}{\sqrt{|a|^2+1}}, \quad \beta = \frac{\mathrm{Re}(a)}{\sqrt{|a|^2+1}}, \quad \phi = \arg(a) \tag{6}$$

Eigen-polarization states calculated from the simulated transmission are shown in the insets in Figure 2c. At the resonant frequency of 140 THz, these eigen-polarization states are nonorthogonal counter-rotating elliptically polarized waves. In contrast, the eigen-polarization states are nearly orthogonal in other frequencies such as 105 and 225 THz, and here the metamaterial shows symmetric transmission spectra. In fact, they are not orthogonal if and only if the asymmetric transmission is nonzero, since the inner product of the two states is

$$e_1^+ e_2 = \left(\alpha\ \beta e^{-i\phi}\right)\begin{pmatrix} \alpha \\ -\beta e^{i\phi} \end{pmatrix} = \frac{|B|-|C|}{|B|+|C|} \tag{7}$$

For backward propagation, the bilayer half-gammadion metamaterial has different eigen-polarization states: $(\pm\beta\ \exp(-i\phi)\ \alpha)^T$. Except for the negative sign of the phase, which is a consequence of a coordinate change, they coincide with $R_y(\pi)R_z(\pi/2)$ transformed image of the eigen-polarization states of the forward case. It accords with the fact that the proposed metamaterial design is invariant under $R_y(\pi)R_z(\pi/2)$. Since two eigen-polarization states of the metamaterial design are $R_y(\pi)$ images of each other, eigen-polarization states of backward propagation are identical to the $\pi/2$ rotated image of those of forward propagation along the *z*-axis. Therefore, if two eigen-polarization states of forward propagation are orthogonal, a set

of eigen-polarization states of forward and that of backward propagation are identical. In such a case, transmission is symmetric for both forward and backward propagations since the two cases are optically identical. Meanwhile, symmetric transmission ensures orthogonality of eigen-polarization states from Equation (7). Thus, the transmission of forward and backward propagations is symmetric if and only if a set of eigen-polarization states are orthogonal. This equivalence explains why eigen-polarization states of asymmetric transmission range are nonorthogonal.

We can better understand the underlying mechanism of the asymmetric transmission from a microscopic dipole picture. Starting with optical responses of a single layer, transmission through the two layers, neglecting the coupling between them, will be described. Then, we will discuss how the interaction between the two layers affects the asymmetric transmission. Each half-gammadion structure has a long bar and two short side bars at the ends. They function as two orthogonal dipoles[35,36] affecting the scattered field by absorbing incident waves and re-emitting different polarization components. The long bar and side bars act as dipoles that interact strongly and weakly with the incident field parallel to the bar orientation, respectively, at the working frequency range. Transmittance spectra of the single bottom layer (**Figure 3**a) show pronounced coupling between the half-gammadion structure and *y*-polarized incidence, because the electric field excites the long bar strongly. This results in nearly zero *y*-polarized waves in transmission close to the frequency of 150 THz. However, for *x*-polarized incidence, the lower layer interacts weakly, transmitting most of the *x*-polarized waves and converting some part of the *x*-polarized field into *y*-polarization. The cross-polarization coefficients (T_{xy} and T_{yx}) of the single layer are identical because of the symmetry along the propagation direction.

Although optical responses of the structure come from hybridized mode of two layers, Jones matrix of the bilayer structure shows similar tendency by multiplying the Jones matrix of the lower and upper layers as shown in Figure 3c,d. Since a single layer itself is symmetric along the propagation axis, Jones matrix of the lower layer has the form as $\begin{pmatrix} P & Q \\ Q & R \end{pmatrix}$, in which the off-diagonal elements are identical. Then Jones matrix of the upper layer is $\begin{pmatrix} R & Q \\ Q & P \end{pmatrix}$, based on the geometric symmetry between the two layers. If we assume the interlayer coupling is weak, Jones matrix of the bilayer half-gammadion structure for forward propagation is given by

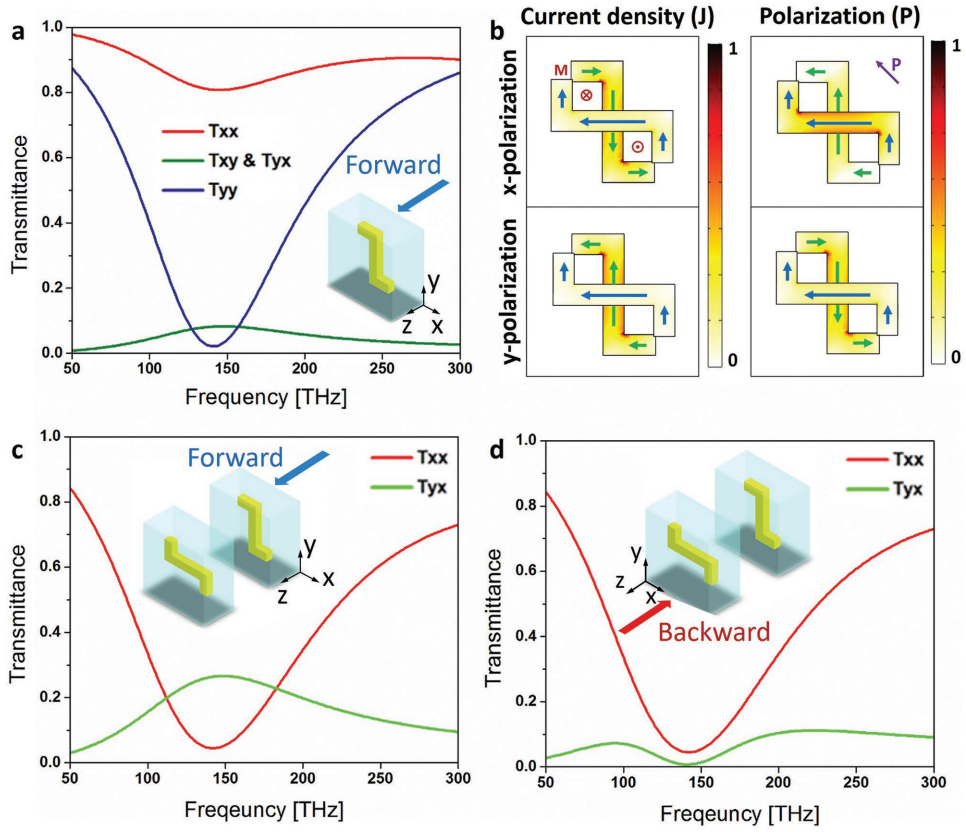

Figure 3. a) Transmittance spectra of the bottom layer. b) Normalized current density and polarization distribution of forward propagation. Color map describes the amplitude of each quantity vector, and arrows show its direction. Blue and green arrows correspond to the top and bottom layers, respectively. Red circles enclosing a cross and a dot in the top left panel indicate the direction of induced magnetization, and purple arrows in the top right panel show the direction of induced polarization. Transmittance spectra of bilayer assuming no interaction between two layers for c) forward and d) backward propagations. Despite the neglected interaction between two layers, the transmittance characteristic shows similar tendency with the original device.

$$\begin{pmatrix} R & Q \\ Q & P \end{pmatrix}\begin{pmatrix} P & Q \\ Q & R \end{pmatrix} = \begin{pmatrix} PR+Q^2 & 2QR \\ 2PQ & PR+Q^2 \end{pmatrix} \quad (8)$$

while that of backward propagation is

$$\Lambda^{-1}\begin{pmatrix} P & Q \\ Q & R \end{pmatrix}\begin{pmatrix} R & Q \\ Q & P \end{pmatrix}\Lambda = \begin{pmatrix} PR+Q^2 & -2PQ \\ -2QR & PR+Q^2 \end{pmatrix}, \quad \Lambda = \begin{pmatrix} 1 & 0 \\ 0 & -1 \end{pmatrix} \quad (9)$$

Here Λ is added to take care of different coordinate convention in backward propagation. Equations (8) and (9) show asymmetric transmission characteristic, which stems from the reverse order of dipole excitation. In short, transmission is dependent on the propagation direction because waves propagating along the forward and backward directions experience different dipoles in different order.

The overall good agreement between this approach and direct full-wave simulation shown in Figure 2 implies that coupling between two layers is weak. However, there is a notable difference of T_{yx} coefficient near 140 THz in Figure 3c,d compared to Figure 2 a,b. The reason is that the relative high value of T_{yx} is originated from the inter-layer coupling. To examine the physical mechanism of the discrepancy, we calculated current density and polarization, which are two fundamental quantities to show electromagnetic resonances. Normalized current density and polarization at 140 THz are shown in Figure 3b. Under *y*-polarized incidence, the current density and polarization of lower and upper layers cancel each other and do not produce net magnetization and polarization. On the other hand, under *x*-polarized incidence, the current density and polarization of the upper layer induced by the fields of the lower layer are in phase with those generated in the upper layer from the incident fields. As a consequence, the in-phase responses result in nonzero electric and magnetic dipoles, and the reradiated waves from the induced dipole moments enhance cross-polarization conversion ratio. Note that the asymmetric transmission takes place in a relatively wider frequency range as shown in Figure 3, compared with the results in Figure 2 in which the inter-layer coupling is included.

Since the structure has nanoscale feature size, some imperfections during fabrication processes are inevitable. Therefore, we have examined asymmetric transmission of the misaligned devices, which shows remarkable robustness of the design. We can understand the excellent tolerance of our device in the following way. From the effective medium theory, each layer of the half-gammadion structures may be characterized as a homogeneous thin film with effective permittivity and permeability. Then the whole structure can be considered as two effective thin films embedded in a silica material. As a result, the relative translational offset between the realistic, bilayer half-gammadion structures is expected to have negligible influence on the optical response. This

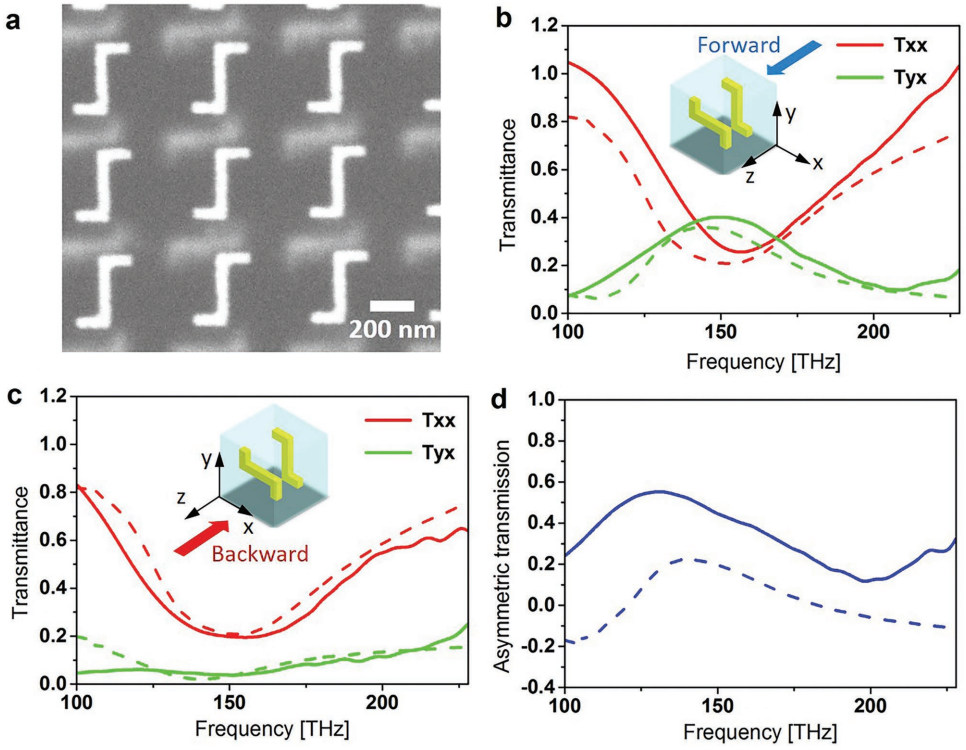

Figure 4. a) SEM image of the fabricated device with translational error of ≈200 nm in the *y*-direction. Measured transmittance of the device for b) forward propagation and c) backward propagation. d) The contrast of asymmetric transmission. Both transmittance spectra and asymmetric transmission keep their original features even under the large spatial misalignment. Solid and dashed lines indicate the characteristics of the misaligned and well-aligned devices, respectively.

intuitive picture is fully supported by the numerical simulations of the dependence of our design on various types of errors as shown in Figure S1 in the Supporting Information. Here, we experimentally verify the design robustness by measuring transmittance spectra of the device in which we deliberately introduce 200 nm of misalignment in the *y*-direction. The SEM image and FTIR measurement results are plotted in **Figure 4**. Figure 4b,c demonstrates that the transmittance in both forward and backward propagation directions of the misaligned device (solid lines) does not present any notable differences compared with the original well-aligned device. Asymmetric transmission shown in Figure 4d proves high flexibility of our device in implementing in applications. Therefore, we can confirm that, regardless of the alignment of the top and bottom structures, asymmetric transmission contrast up to 0.6 over a broad bandwidth of 50 THz is obtained.

In conclusion, we numerically and experimentally demonstrate broadband asymmetric transmission for linearly polarized light using a symmetry-breaking metamaterial where the half-gammadion layers work as nanoantennas to interact with incident waves. Since the metamaterial shown here breaks symmetry in the propagation direction, different dipole interactions generate polarization conversions and ultimately asymmetric transmission along the forward and backward directions. We also verify through numerical simulations and experiments that the design is extremely robust under misalignment errors which are unavoidable in fabrication, showing its high compatibility with further practical applications. Moreover, since the design provides asymmetric transmission for only linearly polarized light, but not for circularly polarized one, it will provide additional degrees of freedom in designing photonics devices. Our results will enable many potential applications including, but not limited to, suppressing interferences and interactions in microscale or nanoscale devices and realizing photonic integrated circuits as well as on-chip photonic isolators and circulators.

Supporting Information

Supporting Information is available from the Wiley Online Library or from the author.

Acknowledgements

M.K. and K.Y. contributed equally to this work. J.R. acknowledges the financial support by Young Investigator program (NRF-2015R1C1A1A02036464), Engineering Research Center program (NRF-2015R1A5A1037668) and Global Frontier program (CAMM-2014M3A6B3063708), and M.K & I.K. acknowledge the Global Ph.D. Fellowships (NRF-2017H1A2A1043204 & NRF-2016H1A2A1906519) through the National Research Foundation of Korea (NRF) grant funded by the Ministry of Science, ICT and Future Planning (MSIP) of Korean government. Y.L. acknowledges the financial support from the Office of Naval Research under award number N00014-16-1-2049.

Conflict of Interest

The authors declare no conflict of interest.

Keywords

3D nanostructures, asymmetric transmission, metadevices, metamaterials, optical diodes

Received: June 25, 2017
Published online: August 7, 2017

[1] L. Bi, J. Hu, P. Jiang, D. H. Kim, G. F. Dionne, L. C. Kimerling, C. A. Ross, *Nat. Photonics* **2011**, *5*, 758.
[2] Z. Wang, Y. Chong, J. D. Joannopoulos, M. Soljacic, *Nature* **2009**, *461*, 772.
[3] S. Lepri, G. Casati, *Phys. Rev. Lett.* **2011**, *106*, 164101.
[4] Z. Yu, S. Fan, *Nat. Photonics* **2009**, *3*, 91.
[5] H. Lira, Z. Yu, S. Fan, M. Lipson, *Phys. Rev. Lett.* **2012**, *109*, 033901.
[6] V. Fedotov, P. Mladyonov, S. Prosvirnin, A. Rogacheva, Y. Chen, N. Zheludev, *Phys. Rev. Lett.* **2006**, *97*, 167401.
[7] R. Ji, S.-W. Wang, X. Liu, W. Lu, *Nanoscale* **2016**, *8*, 8189.
[8] A. S. Schwanecke, V. A. Fedotov, V. V. Khardikov, S. L. Prosvirnin, Y. Chen, N. I. Zheludev, *Nano Lett.* **2008**, *8*, 2940.
[9] C. Pfeiffer, C. Zhang, V. Ray, L. J. Guo, A. Grbic, *Phys. Rev. Lett.* **2014**, *113*, 023902.
[10] R. Singh, E. Plum, C. Menzel, C. Rockstuhl, A. K. Azad, R. A. Cheville, F. Lederer, W. Zhang, N. I. Zheludev, *Phys. Rev. B* **2009**, *80*, 153104.
[11] A. V. Novitsky, V. M. Galynsky, S. V. Zhukovsky, *Phys. Rev. B* **2012**, *86*, 075138.
[12] J. Xu, C. Cheng, M. Kang, J. Chen, Z. Zheng, Y.-X. Fan, H.-T. Wang, *Opt. Lett.* **2011**, *36*, 1905.
[13] C. Zhang, C. Pfeiffer, T. Jang, V. Ray, M. Junda, P. Uprety, N. Podraza, A. Grbic, L. J. Guo, *Laser Photonics Rev.* **2016**, *10*, 791.
[14] A. E. Serebryannikov, E. Ozbay, *Opt. Express* **2009**, *17*, 13335.
[15] T. Xu, H. J. Lezec, *Nat. Commun.* **2014**, *5*, 4141.
[16] J. Shi, X. Liu, S. Yu, T. Lv, Z. Zhu, H. F. Ma, T. J. Cui, *Appl. Phys. Lett.* **2013**, *102*, 191905.
[17] M. Kang, J. Chen, H.-X. Cui, Y. Li, H.-T. Wang, *Opt. Express* **2011**, *19*, 8347.
[18] M. Mutlu, A. E. Akosman, A. E. Serebryannikov, E. Ozbay, *Opt. Express* **2011**, *19*, 14290.
[19] M. Mutlu, A. E. Akosman, A. E. Serebryannikov, E. Ozbay, *Phys. Rev. Lett.* **2012**, *108*, 213905.
[20] C. Huang, Y. Feng, J. Zhao, Z. Wang, T. Jiang, *Phys. Rev. B* **2012**, *85*, 195131.
[21] C. Menzel, C. Helgert, C. Rockstuhl, E. B. Kley, A. Tünnermann, T. Pertsch, F. Lederer, *Phys. Rev. Lett.* **2010**, *104*, 253902.
[22] Z. Li, S. Chen, C. Tang, W. Liu, H. Cheng, Z. Liu, J. Li, P. Yu, B. Xie, Z. Liu, J. Li, J. Tian, *Appl. Phys. Lett.* **2014**, *105*, 201103.
[23] C. Lu, X. Hu, H. Yang, Q. Gong, *Opt. Lett.* **2011**, *36*, 4668.
[24] Y. Zhang, D. Li, C. Zeng, Z. Huang, Y. Wang, Q. Huang, Y. Wu, J. Yu, J. Xia, *Opt. Lett.* **2014**, *39*, 1370.
[25] C. He, X.-C. Sun, X.-P. Liu, M.-H. Lu, Y. Chen, L. Feng, Y.-F. Chen, *Proc. Natl. Acad. Sci. USA* **2016**, *113*, 4924.
[26] Ł. Zinkiewicz, J. Haberko, P. Wasylczyk, *Opt. Express* **2015**, *23*, 4206.
[27] L. Feng, M. Ayache, J. Huang, Y.-L. Xu, M.-H. Lu, Y.-F. Chen, Y. Fainman, A. Scherer, *Science* **2011**, *333*, 729.
[28] S. Fan, R. Baets, A. Petrov, Z. Yu, J. D. Joannopoulos, W. Freude, A. Melloni, M. Popović M. Vanwolleghem, D. Jalas, M. Eich, M. Krause, H. Renner, E. Brinkmeyer, C. R. Doerr, *Science* **2012**, *335*, 38.

[29] Y.-L. Xu, L. Feng, M.-H. Lu, Y.-F. Chen, *Phys. Lett. A* **2012**, *376*, 886.
[30] L. Cong, W. Cao, X. Zhang, Z. Tian, J. Gu, R. Singh, J. Han, W. Zhang, *Appl. Phys. Lett.* **2013**, *103*, 171107.
[31] N. K. Grady, J. E. Heyes, D. R. Chowdhury, Y. Zeng, M. T. Reiten, A. K. Azad, A. J. Taylor, D. A. R. Dalvit, H.-T. Chen, *Science* **2013**, *340*, 1304.
[32] R. C. Jones, *J. Opt. Soc. Am.* **1941**, *31*, 488.
[33] C. Menzel, C. Rockstuhl, F. Lederer, *Phys. Rev. A* **2010**, *82*, 053811.
[34] H. A. Lorentz, *Versl. K. Akad. Wet. Amsterdam* **1896**, *4*, 176.
[35] M. Born, *Ann. Phys.* **1918**, *55*, 177.
[36] W. Kuhn, *Z. Phys. Chem., Abt. B* **1933**, *20*, 325.